Curl-free pressure gradients over orography in a solution of the fully compressible Euler equations with long time-steps

HILARY WELLER *

Meteorology, University of Reading, RG4 7AN, UK

AVA SHAHROKHI

Engineering, University of Leeds, LS2 9JT, UK

ABSTRACT

Long, stable and accurate time-steps are important for models of the atmosphere to enable efficient weather and climate predictions. This has motivated the use of semi-implicit, semi-Lagrangian models. However semi-Lagrangian techniques appears not to be ideal for the next generation of models for modern computers. Some new numerical methods are presented that enable long, stable time-steps without the non-local communication of semi-Lagrangian. Sub time-stepping is used for advection and acoustic and gravity waves are treated implicitly without the need for mean and perturbation variables.

In addition, a new technique for modelling flow over orography using terrain following layers is introduced which guarantees curl-free gradients implying that the pressure gradient term is not a spurious source of vorticity. This mimetic property leads to better hydrostatic balance and better energy conservation. Curl-free gradients are achieved by using the co-variant components of velocity over orography rather than the usual horizontal and vertical components.

Results with advective Courant numbers of up to 2.5 and $N\Delta t$ of up to 10 (where N is the Brunt-Väisälä frequency) are presented. This demonstrates the validity of the sub-cycling of advection and the implicit treatment of gravity waves.

1. Introduction

A few aspects of numerical solution techniques for the equations of motion in the stratified atmosphere are not ideal. Limitations of current techniques are discussed and some alternatives are presented. Some motivation for the present work is:

- Time-steps should be as long as possible without jeopardising accuracy or efficiency, motivating semi-implicit, semi-Lagrangian methods (eg Qian et al. 1998; Davies et al. 2005).
  - However semi-Lagrangian advection usually has some disadvantages. It is either not conservative, not suitable for quasi-uniform grids of the sphere or very expensive and complictated.
  - Techniques for treating gravity waves implicitly seem to be very complicated, requiring all variables to be split into mean and perturbation quantities
- The introduction of orography into stratified atmospheres usually introduces errors (eg Klemp 2011) when using terrain following coordinates.
- There is no ideal placement of thermodynamic variables in the vertical. The Charney-Phillips arrangement does not allow consistent advection of density and potential temperature whereas the Lorenz arrangement admits a spurious computational mode (Arakawa and Konor 1996).

The problems are discussed in more detail in this introduction and some possible solutions are presented in the remainder of the paper. An additional motivation for this work is to find numerical methods with the desirable properties of the best weather and climate forecasting models that do not rely on structured grids with all points lining up in the vertical.

a. Solution of Fully Compressible Euler Equations

The fully compressible, rotating Euler equations in flux form (and advective form for entropy) with the equation of state are:

$$\frac{\partial \rho \mathbf{u}}{\partial t} + \nabla \cdot \rho \mathbf{u}\mathbf{u} + 2\rho\Omega \times \mathbf{u} = \rho \mathbf{g} - c_p \rho \theta \nabla \Pi \tag{1}$$

$$\frac{\partial \rho}{\partial t} + \nabla \cdot \rho \mathbf{u} = 0 \tag{2}$$

$$\frac{\partial \rho \theta}{\partial t} + \nabla \cdot \rho \mathbf{u} \theta = 0 \tag{3}$$

$$\frac{\partial \theta}{\partial t} + \mathbf{u} \cdot \nabla \theta \tag{4}$$

$$\Pi^{\frac{1-\kappa}{\kappa}} = \frac{R}{p_0} \rho \theta \tag{5}$$

where ρ is the density, $\mathbf{u}$ is the velocity, Ω is the rotation rate of the planet, $\mathbf{g}$ is the acceleration due to gravity, c_p is the heat capacity at constant pressure, $\theta = T\left(\frac{p_0}{p}\right)^{\kappa}$ is the potential temperature, T is the temperature, p is the pressure, p_0 is a reference pressure, $\Pi = \left(\frac{p}{p_0}\right)^{\kappa}$ is the Exner function of pressure and $\kappa = \frac{R}{c_p} = \frac{c_p - c_v}{c_p} = 1 - \frac{1}{\gamma}$ is the ratio of the gas constant to the heat capacity. Both forms of the entropy equation will be discussed and used.

The fully compressible equations support sound, Lamb and gravity waves which travel much faster than the wind but do not carry much energy and so various approaches have been developed to allow long time-steps relative to these wave speeds:

- Semi-implicit treatment of sound, Lamb and gravity waves in 3D (Tanguay et al. 1990; Cullen 1990; Qian et al. 1998; Janjic et al. 2001; Davies et al. 2005)
- Semi-implicit treatment of acoustic waves in 3D with explicit treatment of gravity waves (Kwizak and Robert 1971; Tapp and White 1976; Benacchio et al. 2014)
- Horizontally explicit, vertically explicit (HEVI) which can be split up further into:
  - Pure HEVI in which no sub-steps are taken (eg Gassmann 2013)
  - Split-explicit in which horizontally propagating fast waves are treated using a smaller sub-time-step (Durran and Klemp 1983; Klemp et al. 2007; Satoh et al. 2008).

  HEVI approaches are efficient due to the high resolution in the vertical relative to the horizontal in models of the atmosphere implying that vertically implicit will give most gain or order to avoid CFL restrictions.

The advantage of the semi-implicit techniques is that long time-steps can be taken, especially if gravity waves are also treated implicitly and advection is calculated using the semi-Lagrangian method (eg Qian et al. 1998; Davies et al. 2005). However for the implicit solution, global, 3D matrix equations must be assembled and solved at every time-step. HEVI and split-explicit approaches avoid the need for a 3D global matrix solution at the cost of much smaller time-steps or sub time-steps. Steppeler et al. (2003) wrote an excellent review of numerical methods for non-hydrostatic models discussing the advantages and disadvantages of different time-stepping and spatial schemes.

There are many simplifications of the Euler equations for meteorological modelling that promise simpler, more efficient models, such as using the hydrostatic approximation (eg White 2003) or solving anelastic or pseudo-incompressible equations (eg Smolarkiewicz and Szmelter 2011). However (dependent on the solution algorithm) these approximations do not lead to large model efficiency gains whereas solution of the fully compressible Euler equations can lead to more stable solutions (eg Janjic et al. 2001). The anelastic approximation has been shown not to be good for large scale dynamics but the pseudo incompressible approximation appears to be a very good approximation (eg Smolarkiewicz et al. 2013; Benacchio et al. 2014). When solving a simplified equation set such as the Boussinesq, anelastic or pseudo-incompressible equations, there is no choice but to solve a 3D elliptic problem, since, for example, the anelastic approximation is equivalent to taking the limit of an infinite speed of sound (Smolarkiewicz et al. 2001). However there is no clear evidence that these approximations lead to simpler code or solutions with lower computational cost. The hydrostatic approximation leads to code that is between 20% faster (Janjic et al. 2001) and a factor of 2 faster (for the ECMWF IFS, Nils, Wedi, personal communication, 2013). HEVI solution techniques can be used to solve fully compressible or hydrostatic equations but not anelastic or pseudo-incompressible.

The semi-implicit method including implicit treatment of gravity waves, as described by Cullen (1990); Tanguay et al. (1990), involves separating the thermodynamic variables into hydrostatically balanced and perturbation variables. An expression for the perturbation potential temperature, θ', is found from the advective form entropy equation and this is substituted into the bouyancy and pressure gradient terms of the vertical momentum equation. The momentum equation, continuity equation and a linearised version of the equation of state are then combined to form a Helmholtz equation for the perturbation Exner function, Π'. The use of hydrostatically balanced reference profiles which are uniform in time and in the horizontal directions leads to cancellation of various terms which consequently simplifies the algorithm. But the perturbation parts can be large and as consequence, if linearisation assumptions are made, these will not always be accurate.

In order to avoid large deviations from reference profiles, Davies et al. (2005) and Melvin et al. (2010) use a reference profile consisting of the profile from the previous time step and so the profile about which the model is linearised is no longer in hydrostatic balance. This means that fewer approximations are made but the semi-implicit technique is more complicated. In their approach, a discretised form of the advective form of the entropy equation (4) for θ is substituted into the pressure gradient term of the vertical velocity equation, $c_p \theta \partial \Pi / \partial z$, thus replacing θ with the vertical velocity, $w = -\mathbf{u} \cdot \hat{\mathbf{g}}$. This leads to

a non-linear pressure gradient term with two terms to be treated implicitly (w and Π). This term, and the equation of state, require linearisation by separating variables into mean and perturbation quantities. This, in combination with the semi-Lagrangian discretisation, allows long time-steps but makes the description of the technique complicated. The description of the semi-implicit, semi-Lagrangian (SISL) algorithm employed by Qian et al. (1998) is also very complicated and we conjecture that the semi-implicit solution of the fully compressible equations has not been taken up widely because these descriptions are so complicated.

Semi-implicit solution techniques including implicit gravity waves using mean state and perturbation variables are also described by (Smolarkiewicz et al. 2001; Smolarkiewicz and Szmelter 2011). In order to move away from the complication of using mean and perturbation variables, Benacchio et al. (2014) describe a method of treating sound but not gravity waves implicitly in which a blend between fully compressible and pseudo-incompressible dynamics can be made. This involves combining the flux form of the potential temperature equation with the momentum equation but the continuity equation is solved separately, thus avoiding a linearisation of the equation of state.

In this paper, we will describe a method of treating acoustic and gravity waves implicitly without a reference profile or perturbation variables. The continuity, entropy and momentum equations are combined using the exact equation of state but with some terms defined from a previous iteration. Test cases using a large $N\Delta t$ (where N is the Brunt-Väisälä frequency) demonstrate the stability for fast gravity waves. The techniques described do not make any assumptions about the structure of the grid or the direction of gravity but all test cases use structured grids with gravity aligned with the z direction which is aligned with grid lines. Test using different grid structures are under way but not reported here.

b. Treatment of Orography

Weather and climate forecasting models use terrain following coordinates so that the grid does not intersect with the ground, grid boxes are arranged exactly in vertical columns and high resolution of the planetary boundary layer is maintained. The prognostic velocity variables are usually the vertical velocity and two components of horizontal velocity. In order to solve the components of the momentum equation, the pressure gradient is needed in the same direction as the velocity components. This is straightforward for the vertical velocity because the prognostic pressure variables will also be aligned in vertical columns and so the vertical pressure gradient, $\partial\Pi/\partial z$, will be straightforward to calculate accurately. However, around steep orography, $\nabla_h\Pi = (\partial\Pi/\partial x, \partial\Pi/\partial y, 0)$ will be more difficult to calculate because Π is not known along constant horizontal surfaces but along terrain following surfaces. Consequently, much work has gone into accurate evaluations of $\partial\Pi/\partial x$ using Π data from different layers (eg Zängl 2012). However these methods are never as accurate as calculating $\partial\Pi/\partial x$ from data all at the same height (Good et al. 2013) and therefore there has also been work into creating terrain following coordinates that become smooth rapidly above mountains (eg Schär et al. 2002; Klemp 2011) and into using height coordinates that intersect with the ground and consequently have cut cells adjacent to the orography (Adcroft et al. 1997; Bonaventura 2000; Steppeler et al. 2002)

The common approach of using vertical and horizontal velocity components as prognostic variables with terrain following coordinates implies that the vertical velocity is a covariant component of the velocity whereas the horizontal velocity is a contravariant component. On horizontal non-orthogonal grids, regardless of using Arakawa B or C grids (Rančić et al. 1996; Adcroft et al. 2004; Thuburn et al. 2013; Weller 2013), the CD grid (Putman 2007; Harris and Lin 2013) or discontinuous Galerkin (Nair et al. 2005), the covariant velocity is used as the prognostic variable. In this paper, we will explore the use of covariant velocity components as prognostic variables in combination with terrain following meshes in Cartesian space. This will enable calculation of pressure gradients which are curl-free (Thuburn and Cotter 2012) thus ensuring that the pressure gradient term of the momentum equation is not a spurious source of vorticity.

c. Vertical Staggering and form of the Entropy Equation

The Lorenz arrangement of variables has (Exner function of) pressure, Π, and (potential) temperature, θ, co-located which are staggered from vertical velocity, w, whereas Charney-Phillips has θ at the same level as w, staggered from Π (Arakawa and Konor 1996). The Lorenz grid has a computational mode consisting of grid-scale vertical θ oscillations which are spuriously in hydrostatic balance. The Charney-Phillips arrangement has been shown to be advantages in many applications, including the simulation of baroclinic instability (Arakawa and Moorthi 1988) and hurricane simulation (Zhu and Smith 2003). However the Lorenz grid remains popular because it is more straightforward to have all thermodynamic variables in the same location, making energy conservation simpler to achieve (Holdaway et al. 2013) and enabling consistent transport of ρ and θ. Using the Lorenz grid, the entropy equation (3) can be solved in flux form, with the horizontal and vertical fluxes staggered from θ in an arrangement like an Arakawa C-grid in the vertical. However, if θ and w are co-located, fluxes would have to be interpolated to solve the entropy equation in flux form. It is therefore more natural to solve the advective form of the entropy equation (4) when using Charney-Phillips vertical staggering. This form will also admit computational modes since the horizontal components of the velocity must be averaged to θ levels for calculating $\mathbf{u}\cdot\nabla\theta$. However this problem has not been discussed in the literature. The advective form also makes it more straightforward to treat gravity waves implicitly, since $\mathbf{u}$ is outside a differential operator and so θ can be substituted for $\mathbf{u}$ in the pressure gradient term of the momentum equation, $c_p\rho\theta\nabla\Pi$.

In this paper we use Lorenz staggering in order to achieve consistent transport of ρ and θ and energy conservation in a form that will work on three dimensionally unstructured meshes

(although these are not tested). However, in order to treat gravity waves implicitly, the advective form of the entropy equation is used within the iterations of a full time-step.

d. Implicit/Explicit (IMEX) Time-Stepping

Implicit and explicit time-stepping schemes have long been combined in models of the atmosphere. For example, the semi-implicit technique (Tapp and White 1976) involves treating fast waves implicitly and slower waves and advection explicitly whereas split-explicit and other horizontally explicit, vertically implicit techniques involve treating vertically propagating sound waves implicitly and all horizontally varying terms explicitly (eg Cullen and Davies 1991; Skamarock and Klemp 1992). Runge-Kutta IMEX schemes, provide a stable and high order technique for combining implicit and explicit time-stepping techniques (eg Pareschi and Russo 2005) and recently, these techniques have been analysed and applied to wave equations, making them suitable for atmospheric modelling (Ullrich and Jablonowski 2012; Lock et al. 2013; Weller et al. 2013). Runge-Kutta IMEX schemes have previously been defined and analysed for two different time-stepping schemes, one fast and one slow. However for atmospheric modelling we are concerned with more than two time scales. Acoustic and gravity waves can be considered fast in comparison to advection. But the non-linearities of the wave equations cannot be treated implicitly but should be treated with similar time-step weights to the linear terms. We will therefore define, analyse and use an implicit/explicit/explicit Runge-Kutta time-stepping scheme (RK IMEXEX), with a third-order, strong stability preserving explicit scheme for advection.

e. Outline of this Paper

The article describes a new discretisation of the fully compressible Euler equations suitable for strongly stratified flow over orography. The discretisation has exactly curl-free pressure gradients implying that the pressure gradient term is not a spurious source of vorticity and both acoustic and gravity waves are treated implicitly, which allows longer stable time-steps. The formulation does not use an explicitly defined reference profile or perturbation variables which makes it simpler and enables more clarity in ensuring conservation properties. The numerical method is described in section 2 and some test cases and results demonstrating the properties of the method are presented in section 3.

2. Numerical Method

The numerical method comprises:

i. Solution of the non-linear, fully compressible Euler equations in flux form.

ii. Semi-implicit treatment of acoustic and gravity waves.

iii. No explicitly defined reference profile and no reliance on perturbation variables.

iv. Exact conservation of mass

v. Curl-free pressure gradients over orography.

vi. A split space-time (method of lines) multi-dimensional quadratic upwind advection scheme.

vii. Lorenz staggering of θ and Π (With some Charney-Phillips elements within each time-step).

viii. A combination of one implicit and two explicit Runge Kutta time-stepping schemes (RK IMEXEX). These are:

   (a) Trapezoidal implicit for the linearised fast terms.

   (b) Mid-point for the non-linearities of the fast terms

   (c) A third-order, strong stability preserving (SSP) RK scheme for the non-linear advection.

   The SSP RK scheme is combined with the others using Strang splitting.

ix. The C-grid finite volume method for spatial discretisation.

This numerical method has been implemented using OpenFOAM (cited 2013). The implementation described in this paper can be downloaded from `http://www.met.rdg.ac.uk/~sws02hs/ExnerFoam`.

a. Spatial Discretisation and Placement of Prognostic Variables

The spatial discretisation is C-grid staggered finite volume with Lorenz staggering of thermodynamic variables. The discretisation of the Coriolis term is not described here as none of the test-cases presented in section 3 have rotation.

1) NOTATION

A variable, ψ, located at a cell centre is given subscript c: ψ_c where c is the cell number. A variable, ψ, located on a face between cells is given subscript f where f is a face number. A variable without a subscript implies an array of all of the cell or face values over the entire mesh. Interpolation of cell centre values to face values is denoted with subscript F: ψ_F. Reconstruction of cell values from face values is denoted with subscript C: ψ_C. $f \in c$ means the faces of cell c and $c \in f$ means the (2) cells either side of face f.

2) PROGNOSTIC VARIABLES

The prognostic variables are the cell centre Exner function, Π_c, the cell centre potential temperature, θ_c (hence Lorenz staggering) and the momentum at the cell faces in the cell centre to cell centre direction, $V_f = \rho \mathbf{u} \cdot \mathbf{d}_f$ where the vector $\mathbf{d}_f$ is defined for each face and is the vector between the cell centres on either side of the face. These variables and vectors are shown in figure 1.

In order to solve the continuity equation using Gauss's divergence theorem, we will also need the mass flux over every

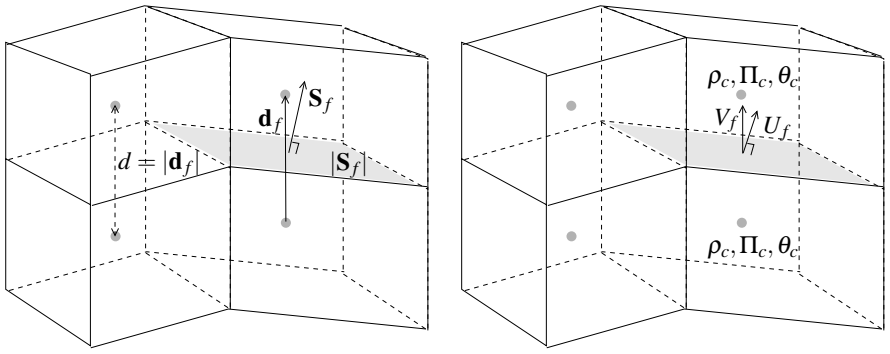

(a) Geometry (b) Placement of variables

FIG. 1. Geometric vectors $\mathbf{S}_f$ (face area vector, normal to the face with magnitude of the face area) and $\mathbf{d}_f$ (the vector between adjacent cell centres) and cell centre position of prognostic variables Π_c and θ_c and diagnostic variable ρ_c, face locations of momentum components, $U_f = \rho\mathbf{u}\cdot\mathbf{S}_f$ and $V_f = \rho\mathbf{u}\cdot\mathbf{d}_f$.

cell face as a diagnostic variable. This is denoted $U = \rho\mathbf{u}\cdot\mathbf{S}$ where face area vector, $\mathbf{S}$ is normal to each face with magnitude of the face area. In order to find the field of Us from the field of Vs we need operator H:

$$U = HV$$

which is defined in Weller (2013). Here we use the asymmetric version of H which does not guarantee energy conservation but can be generalised to three dimensions. The use of V (covariant momentum component) rather than U (contravariant component) as a prognostic variable was recommended by Thuburn and Cotter (2012) in order to achieve a combination of mimetic properties, including curl-free pressure gradients and conservation of energy.

3) SPATIAL DISCRETISATION

None of the spatial discretisation described assumes a structured grid and the implementation is for an arbitrarily structured 3D grid. However all of the test cases described in section 3 use 2D, terrain following, structured grids.

(i) Gradients

For a cell centred, scalar field, Ψ, two different types of gradients are defined. For the C-grid-staggered method with $V = \rho\mathbf{u}\cdot\mathbf{d}$ as the prognostic variable, the gradient at the face in direction $\mathbf{d}$ is required:

$$\nabla_d\Psi = \sum_{c\in f} -n_f\Psi_c \tag{6}$$

where $n_f = 1$ if $\mathbf{S}_f$ points outward from the cell and -1 otherwise. This simple two-point gradient leads to curl-free pressure gradients. For the solution of advective form entropy equation, the gradient at the cell-centre is also needed and is defined using Gauss's theorem:

$$(\nabla\Psi)_c = \frac{1}{V_c}\sum_{f\in c} n_f\Psi_F\mathbf{S}_f \tag{7}$$

where the cell has volume V_c. The interpolation of Ψ from cell centres onto faces to calculate Ψ_F uses a multi-dimensional quadratic least squares fit over an upwind biased stencil of cells which is described in section vi. In general $\mathbf{d}_f\cdot(\nabla\Psi)_F \neq \nabla_d\Psi$ but changes to equality for linearly varying fields. For solving the entropy equation in advective form, the entropy gradient at the face in the plane normal to $\mathbf{d}$ is needed. This is interpolated from the cell centred entropy gradient using arithmetic mean interpolation: $(\nabla\theta)_F = \frac{1}{2}\sum_{c\in f}(\nabla\theta)_c$ and the component in direction $\mathbf{d}$ is not used.

(ii) Divergence

Divergences are calculated at cell centres using Guass's divergence theorem, eg for scalar field Ψ and vector field, $\mathbf{v}$, both defined at cell centres:

$$(\nabla\cdot\Psi\mathbf{v})_c = \frac{1}{V_c}\sum_{f\in c} n_f\Psi_F\mathbf{v}_F\cdot\mathbf{S}_f \tag{8}$$

or, since momentum component $U = \rho\mathbf{u}\cdot\mathbf{S}$ is defined at the face then $\nabla\cdot\rho\mathbf{u} = \frac{1}{V}\sum_{f\in c} n_f U$ which is simply denoted $\nabla\cdot U$. Similarly, $\nabla\cdot\rho\mathbf{u}\Psi = \frac{1}{V}\sum_{f\in c} n_f\Psi_F U$ which is denoted $\nabla\cdot U\Psi$. Again, a multi-dimensional quadratic least squares fit over an upwind biased stencil of cells is used to calculate Ψ_F which is described in section vi. For solving the momentum equation on the face, the non-linear advection term is needed on the face. This is interpolated from the cell centred values using arithmetic mean interpolation: $(\nabla\cdot U\mathbf{u})_F = \frac{1}{2}\sum_{c\in f}(\nabla\cdot U\mathbf{u})_c$.

(iii) Reconstruction of Cell Centre Velocity

Following Weller (2013), cell centre velocity is reconstructed from face fluxes using:

$$\mathbf{u}_C = \left(\sum_{f \in c} \mathbf{d}_f \mathbf{d}_f^T \right)^{-1} \sum_{f \in c} \frac{V_f \mathbf{d}_f}{\rho_F} \tag{9}$$

where $\mathbf{d}_f \mathbf{d}_f^T$ is a 3×3 tensor and so the inversion of the tensor sum is a local operation which can be calculated once for the mesh rather than at each time-step. Equation (9) is a least squares fit which reconstructs uniform vector fields exactly.

(iv) Perpendicular component of momentum

For the implicit treatment of gravity waves using the advective form of the entropy equation, the component of the momentum perpendicular to $\mathbf{d}_f$ is needed:

$$\mathbf{v}_f^{\perp} = (\rho \mathbf{u})_F - \frac{(\rho \mathbf{u})_F \cdot \mathbf{d}_f}{|\mathbf{d}_f|^2} \mathbf{d}_f$$

where $(\rho \mathbf{u})_F$ is calculated using arithmetic mean interpolation.

(v) Interpolations for Lorenz staggering

Using Lorenz staggering, θ, Π and ρ are all calculated and stored at cell centres and, where needed, interpolated onto faces using the arithmetic mean: $\theta_F = \frac{1}{2} \sum_{c \in f} \theta_c$ and $\rho_F = \frac{1}{2} \sum_{c \in f} \rho_c$. However, as will be described in section 1 below, in the course of one time step, θ is also advanced on the face using the advective form of the entropy equation [4]. This is denoted θ_f. At the beginning of the time-step, θ_f is set to θ_F by interpolating from θ but then θ_f is modified during the RK stages. Charney Phillips staggering could be achieved by setting cell-centre θ from θ_f at the beginning of the time-step instead but this has not yet been done.

(vi) Advection of momentum and entropy

The interpolation operations, $\mathbf{u}_F$ and θ_F, in the terms

$$\nabla \cdot U \mathbf{u} = \frac{1}{V} \sum_{f \in c} n_f \mathbf{u}_F U$$

$$\nabla \cdot U \theta = \frac{1}{V} \sum_{f \in c} n_f \theta_F U$$

$$\mathbf{u} \cdot \nabla \theta = \mathbf{u} \cdot \frac{1}{V_c} \sum_{f \in c} n_f \theta_F \mathbf{S}_f$$

control the advection of momentum and entropy and so should be undertaken using an upwind biased interpolation scheme. We have used a least-squares fit to a multi-dimensional quadratic using an upwind-biased stencil of cells (Weller et al. 2009). In two-dimensions, the multi-dimensional quadratic is

$$\Psi = a + bx + cy + dx^2 + exy + fy^2 \tag{10}$$

where coefficients $a - f$ are set from a least squares fit to the cell data in the stencil. The least-squares problem involves a $6 \times m$ matrix inversion for every face where m is the size of the stencil. However this is purely a geometric calculation and is therefore a pre-processing activity since the mesh is fixed. This generates a set of weights for calculating Ψ_F from the cell values in the stencil leaving m multiplies for each face for each call of the advection operator. The stencils are found for three-dimensional, arbitrarily structured meshes by finding the face(s) closest to upwind of the face we are interpolating onto, taking the two cells either side of the upwind face(s) and then taking the cell neighbours of those central cells. For a two-dimensional structured grid, this gives the stencil shown in figure 2.

The advection scheme is not an important part of the algorithm described. Any other advection scheme, monotonic and/or forward in time, could be used instead.

b. Sponge Layer

Following Melvin et al. (2010), a damping term is added to the momentum equation to suppress wave reflections of the rigid lid. This term is $-\mu \rho \mathbf{u}$ where μ is non-zero only for vertical velocities near the model top. The distribution of the sponge layer is:

$$\mu = \begin{cases} 0 & z < z_B \\ \bar{\mu} \sin^2 \frac{\Pi}{2} \frac{z - z_B}{z_t - z_B} & z \geq z_B \end{cases}$$

where $z = -\mathbf{x} \cdot \hat{\mathbf{g}}$ is the distance from position $\mathbf{x}$ to the surface, z_B is the height of the bottom of the sponge layer and z_t is the height of the model top.

c. Runge-Kutta Implicit/Explicit/Explicit time-stepping (RK IMEXEX)

In order to describe the RK IMEXEX time-stepping, we consider solution of the ODE:

$$\frac{dy}{dt} = s(y) + m(y) + f(y)$$

where s leads to slow variations in y and could be non-linear, f is linear and leads to fast variations in y and m is medium and non-linear and so may require sub-stepping. Since there are three terms with different timescales, we will define an IMEXEX (implicit-explicit-explicit) Runge-Kutta scheme inspired by the Strang Carryover scheme of Ullrich and Jablonowski (2012) to go from time level n ($y^{(n)}$) to time level $n+1$ ($y^{(n+1)}$) with time step Δt

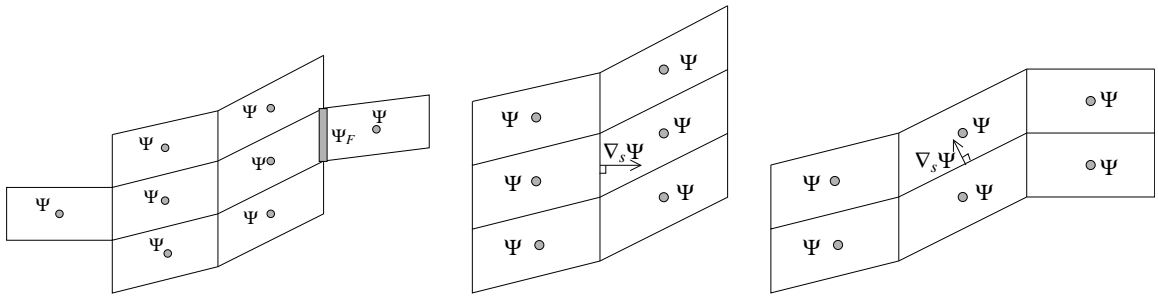

FIG. 2. Finite difference stencils for quadratic upwind advection and calculating $\nabla_s\Psi = \nabla\Psi\cdot\mathbf{S}$, the least squares linear gradient in the horizontal $\mathbf{S}$ direction and the near vertical $\mathbf{S}$ direction.

using M sub time-steps for term m:

$$
\begin{aligned}
y^0 \quad &= y^{(n)} \\
y^1 \quad &= y^{(n)} + (1-\alpha)\Delta t\left(s\left(y^0\right) + f\left(y^0\right)\right) \\
\text{for} \quad & k = 0,\ldots,M-1 \\
&\begin{cases} y^{3k+2} = y^{3k+1} + \frac{\Delta t}{M} m\left(y^{3k+1}\right) \\ y^{3k+3} = y^{3k+2} + \frac{\Delta t}{4M}\left(3m\left(y^{3k+1}\right) - m\left(y^{3k+2}\right)\right) \\ y^{3k+4} = y^{3k+3} + \frac{\Delta t}{12M}\left(m\left(y^{3k+1}\right) + m\left(y^{3k+2}\right) - 8m\left(y^{3k+3}\right)\right) \end{cases} \\
y^{3M+2} &= y^{3M+1} - (1-\alpha)\Delta t s\left(y^0\right) + \Delta t\left(s\left(y^{3M+1}\right) + \alpha f\left(y^{3M+2}\right)\right) \\
y^{(n+1)} &= y^{3M+1} + \alpha\Delta t\left(s\left(y^{3M+2}\right) + f\left(y^{(n+1)}\right)\right)
\end{aligned}
\tag{11}
$$

where variable y represents a vector of all values of all of the prognostic variables. $\alpha = 1/2$ is used which gives second-order Strang splitting (equivalent to Crank-Nicholson or trapezoidal implicit for the fast terms). There is no implicit stage before the SSP RK scheme. This is then Strang carryover (Ullrich and Jablonowski 2012) rather than formal Strang splitting. Strang carryover reduces the cost, retains second-order accuracy and actually improves stability (Lock et al. 2013; Weller et al. 2013). The slow scheme is the 2nd order mid-point scheme which is appropriate to combine with the fast trapezoidal scheme because the slow scheme is used to update the non-linearities and mid-point and trapezoidal can be combined with minimal splitting. The medium scheme is a third order, explicit, SSP RK scheme with sub stepping.

1) IMPLICIT AND EXPLICIT TREATMENT OF DIFFERENT TERMS

The linearised terms involved in acoustic and gravity wave propagation and the sponge layer are treated implicitly. That is, the linearised version of $\theta\nabla\Pi$ and $\mu\rho\mathbf{u}$ in the momentum equation, $\nabla\cdot\rho\mathbf{u}$ in the continuity equation, the $\mathbf{u}$ from $\mathbf{u}\cdot\nabla\theta$ in the advective form of the entropy equation and the θ from $\nabla\cdot\rho\mathbf{u}\theta$ in the flux form of the entropy equation. These terms have superscript f in the equations below to mean "fast". The non-linearities in the fast terms are assumed to be slow, along with $\rho\mathbf{g}$ and are therefore treated explicitly. These have superscript s below. The test cases presented in section 3 do not include rotation and so the discretisation of the Coriolis is not described. The non-linear advection term, $\nabla\cdot\rho\mathbf{u}\mathbf{u}$ is the medium speed term, treated with the SSP RK time-stepping scheme with sub-stepping and is given superscript m below. The Euler equations with superscripts denoting the time-stepping scheme used for each term are:

$$\frac{\partial\rho\mathbf{u}}{\partial t} + \nabla\cdot(\rho\mathbf{u}\mathbf{u})^m = \rho^s\mathbf{g} - \rho^s c_p\theta_f^f\nabla\Pi^f - \mu\rho\mathbf{u}^f \tag{12}$$

$$\frac{\partial\rho}{\partial t} + \nabla\cdot(\rho\mathbf{u})^f = 0 \tag{13}$$

$$\frac{\partial\rho\theta}{\partial t} + \nabla\cdot(\rho\mathbf{u})^f\theta^f = 0 \tag{14}$$

$$\frac{\partial\theta_f}{\partial t} + \mathbf{u}^f\cdot\nabla\theta^s \tag{15}$$

The details of the linearisation and how the implicit terms are combined is given in sections d, e and f.

2) MEMORY CONSIDERATIONS

Although there are numerous different stages, only 2 independent levels need to be stored, $y^{(n)}$ and $y^{(n+1)}$ are stored while y^j over-writes the memory from $y^{(n)}$ for $j = 0,\ldots,3M+1$ and the y^j use the memory from $y^{(n+1)}$ for $j = 3M+2,\ 3M+3$. In addition, $\frac{\Delta t}{M}m\left(y^{3k+1}\right)$ and $\frac{\Delta t}{M}m\left(y^{3k+2}\right)$ need storing but these are smaller fields since they only include the non-linear advection. The other advantage in storing $\frac{\Delta t}{M}m\left(y^{3k+1}\right)$ and $\frac{\Delta t}{M}m\left(y^{3k+2}\right)$ rather than storing y^{3k+1} and y^{3k+2} is that the expensive non-linear advection term does not need to be re-calculated.

These memory requirements hold for variables which are linear in the rate of change term. So these are the requirements for $\rho\mathbf{u}$. However the flux form equation for θ has a rate of change of $\rho\theta$. Therefore $\rho^{(n)}$ and $\theta^{(n)}$ cannot be over-written until the end of the time-step. The same will be true for Π, for which we will form a conservation equation, the Helmholtz equation, with a non-linear rate of change.

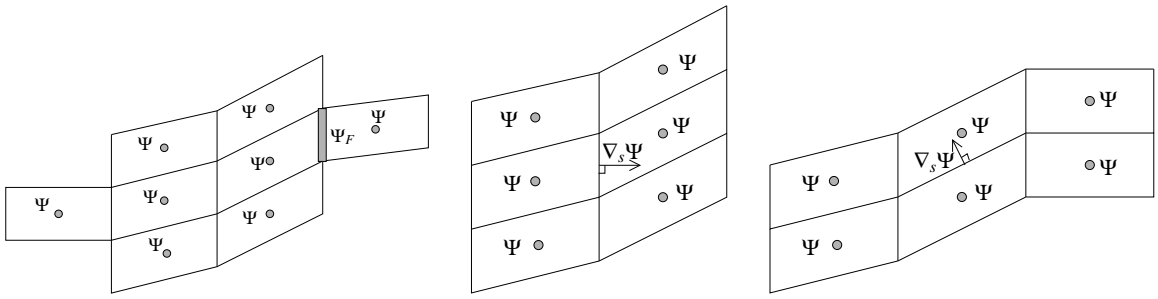

FIG. 3. Amplification factor magnitudes for sovling a wave equation using the combination of fast and slow time-stepping schemes, fast and medium and slow and medium for ranges of fast, medium and slow rates. The numbers show the order of accuracy of the slower scheme, the faster scheme and the combined scheme. The $|A| = 1$ contour is black. White contours every 0.1 up to 1.5

3) STABILITY ANALYSIS OF RK IMEXEX

The linear stability of the combined time-stepping schemes can be analysed using von-Neumann stability analysis as described by Lock et al. (2013); Weller et al. (2013). The linear wave equation

$$\frac{dy}{dt} = isy + imy + ify$$

(with $s, m, f \in \mathscr{R}$ and $i = \sqrt{-1}$) is analysed giving the amplification factor magnitudes as shown in figure 3. The order of accuracy of the schemes and their combinations is calculated as described by Pareschi and Russo (2005). The trapezoidal-implicit and explicit mid-point schemes are second order and the SSP RK scheme is third order. The combination of the mid-point and SSP RK schemes is only first order due to the asymmetry of taking the large mid-point step after the SSP RK scheme. However, for the equations solved, the combination is second order because the non-linear advection (advanced using SSP RK) does not interact with the slow terms. If Coriolis were included and treated as a slow term, the interaction between Coriolis and non-linear advection would be first order. It may therefore be better to treat the Coriolis as a medium or fast term. Or the slow and other schemes should be combined differently. This is not investigated further here.

d. First, explicit (carryover) stage for the Euler equations

In the RK IMEXEX time-stepping scheme, the first substage is

$$y^1 \quad = y^{(n)} + (1-\alpha)\Delta t \left(s\left(y^{(n)}\right) + f\left(y^{(n)}\right)\right).$$

This stage is undertaken for the momentum in direction **d**, the continuity equation and both forms of the entropy equation:

$$V^1 = V^{(n)} + (1-\alpha)\Delta t \left(\rho_F \mathbf{g}\cdot\mathbf{d} - \rho_F c_p \theta_f^{(n)} \nabla_d \Pi^{(n)} - \mu V^{(n)} \right) \tag{16}$$

$$\rho^1 = \rho^{(n)} - (1-\alpha)\Delta t \nabla\cdot U^{(n)} \tag{17}$$

$$\theta^1 = \frac{1}{\rho^1}\left(\rho^{(n)}\theta^{(n)} - (1-\alpha)\Delta t \nabla\cdot\left(U^{(n)}\theta_F \right)\right) \tag{18}$$

$$\theta_f^1 = \theta_F^1 \tag{19}$$

(where θ_F uses arithmetic mean interpolation). At this stage, the boundary conditions of V^1 are set to ensure the correct flow over the boundaries.

e. Non-linear Advection sub-stepping

Next, the non-linear advection term in the momentum equation, $\nabla\cdot\rho\mathbf{uu}$, is evaluated to update V using the SSP RK time-stepping scheme:

$$\begin{aligned}
&U^0 = HV^0 \\
&\text{for } k = 0,\ldots,M-1 \\
&\begin{cases}
V^{3k+2} = V^{3k+1} + \frac{\Delta t}{M}\nabla\cdot\left(U^0\mathbf{u}_C\left(V^{3k+1}/\rho_F^1\right)\right) \\
V^{3k+3} = V^{3k+2} + \frac{\Delta t}{4M}\left(3\nabla\cdot\left(U^0\mathbf{u}_C\left(V^{3k+1}/\rho_F^1\right)\right)\right. \\
\qquad\qquad \left. -\nabla\cdot\left(U^0\mathbf{u}_C\left(V^{3k+2}/\rho_F^1\right)\right)\right) \\
V^{3k+4} = V^{3k+3} + \frac{\Delta t}{12M}\left(\nabla\cdot\left(U^0\mathbf{u}_C\left(V^{3k+1}/\rho_F^1\right)\right)\right. \\
\qquad\qquad +\nabla\cdot\left(U^0\mathbf{u}_C\left(V^{3k+2}/\rho_F^1\right)\right) \\
\qquad\qquad \left. -8\nabla\cdot\left(U^0\mathbf{u}_C\left(V^{3k+3}/\rho_F^1\right)\right)\right).
\end{cases}
\end{aligned} \tag{20}$$

The old time level flux, U^0 is used instead of U^1 because U^0 satisfies continuity. The quadratic upwind fit is used to interpolate $\mathbf{u}_C$ from cells to faces (as described in paragraph vi). The time-step is usually limited by the advective Courant number in

semi-implicit models so the scheme described has sub-stepping of this limiting term. It is necessary to ensure that the non-linear advection term is zero at the rigid boundaries in order to enforce no flow at these boundaries.

f. Final, Trapezoidal Implicit Stages for the Euler equations

The two (or three) final, implicit RK sub-stages, $j = 3M+2,\ 3M+3$, each first involve sequential solutions of the continuity then flux form entropy equations:

$$\rho^j = \rho^1 - \alpha\Delta t \nabla \cdot U^{j-1} \tag{21}$$

$$\theta^j = \frac{1}{\rho^j}\left(\rho^1\theta^1 - \alpha\Delta t \nabla\cdot\left(U^j\theta_F^j\right)\right). \tag{22}$$

and then the construction and solution of the Helmholtz equation for Π^j (and V^j).

1) Construction of Helmholtz Equation

A simultaneous solution in all of the prognostic variables together is needed in order to treat acoustic and gravity waves implicitly. To construct a Helmholtz equation in just one variable (Π^j), the momentum, continuity and entropy equations are combined by hand. First, the entropy equation is substituted into the momentum equation to replace θ_f^j with V^j and then the momentum equation is substituted into the continuity equation to replace V^j with Π^j. Finally, ρ^j must be replaced by Π^j on the left hand side of the continuity equation using a linearisation of the equation of state in order to create a Helmholtz equation for Π^j.

We will now introduce an alternative form of the density. The density can either be advanced from the continuity equation or calculated from the equation of state. The version of density chosen is dependent on whether the density should be consistent with advection or thermodynamics. For constructing the Helmholtz equation we will use the thermodynamic density:

$$\rho_f^j = \left(\Psi^j\Pi^{j-1}\right)_F \tag{23}$$

where $\Psi^j = \left(\rho^j\right)^{\frac{2\kappa-1}{\kappa-1}}\left(\frac{R\theta^j}{p_0}\right)^{\frac{\kappa}{\kappa-1}}$ is defined using the equation of state.

In constructing the Helmholtz equation, it is convenient to first add the explicit parts of the RK sub-stage. This is represented by a half sub-stage. So for $j = 3M+1,\ 3M+2$ in eqn [11]:

$$y^{j-1/2} = y^{j-1} + \alpha\Delta t\ s\left(y^{j-1}\right). \tag{24}$$

The entropy equation is substituted into the momentum equation in order to replace the θ_f in $c_p\rho\theta_f\nabla\Pi$ with V. This cannot readily be done using the flux form of the entropy equation. For the first implicit stage, the advective form of the entropy equation is used to advance θ_f using Charney-Phillips vertical staggering:

$$\theta_f^j = \theta_f^1 - \alpha\Delta t\left(\frac{V^j}{\rho_f^j|\mathbf{d}|^2}\nabla_d\theta^j + \frac{\mathbf{v}^{\perp(j)}}{\rho_F^{(j)}}\cdot\left(\nabla\theta^{(j)}\right)_F\right) \tag{25}$$

For the final implicit stage, for energy conservation of the continuous equations, the θ_f in the pressure gradient term should be the same as the θ used in the equation of state. Therefore the following is used:

$$\theta_f^j = \theta_F^j - \alpha\Delta t\frac{V^j}{\rho_f^j|\mathbf{d}|^2}\nabla_d\theta^j + \alpha\Delta t\frac{V^{j-1}}{\rho_f^j|\mathbf{d}|^2}\nabla_d\theta^j \tag{26}$$

which reverts to Lorenz vertical staggering, admitting a computational mode. Equation (25) or (26) is then substituted into the momentum equation. So for the first implicit stage we write:

$$\theta_f^{j-1/2} = \theta_f^1 - \alpha\Delta t\frac{\mathbf{v}^{\perp(j)}}{\rho_F^{(j)}}\cdot\left(\nabla\theta^{(j)}\right)_F \tag{27}$$

and for the final sub-stage:

$$\theta_f^{j-1/2} = \theta_F^j + \alpha\Delta t\frac{V^{j-1}}{\rho_f^j|\mathbf{d}|^2}\nabla_d\theta^j \tag{28}$$

which are calculated explicitly before construction of the Helmholtz equation. Then we have:

$$\theta_f^j = \theta_f^{j-1/2} - \alpha\Delta t\frac{V^j}{\rho_f^j|\mathbf{d}|^2}\nabla_d\theta^j \tag{29}$$

which is substituted into the momentum equation in order to replace θ_f^j in the pressure gradient term with V^j. The momentum equation for the final stages is:

$$V^j = V^{3M+1} + \alpha\Delta t\left(\rho_f^j\mathbf{g}\cdot\mathbf{d} - c_p\rho_f^j\theta_f^j\nabla_d\Pi^j - \mu V^j\right) \tag{30}$$

into which we substitute θ_f^j from equation [26]. This can then be rearranged so that all the terms involving V^j are on the left hand side and some js are replaced by $j-1$s to ensure that the system is linear in j terms:

$$V^j = G\left(V^{3M+1} + \alpha\triangle t\rho_f^j\mathbf{g}\cdot\mathbf{d} - \alpha\Delta t c_p\rho_f^j\theta_f^{j-1/2}\nabla_d\Pi^j\right) \tag{31}$$

where G takes a similar form to that defined by Davies et al. (2005):

$$G = \frac{1}{1-\alpha^2\Delta t^2 c_p\ \nabla_d\theta^j\nabla_d\Pi^{j-1}/|\mathbf{d}|^2 + \alpha\Delta t\mu}. \tag{32}$$

An important note about the implementation is that gravity and pressure gradient terms should cancel exactly on the boundaries even though the gravity term is calculated explicitly and the pressure gradient implicitly. V^j is zero at rigid boundaries and the boundary condition for pressure is $\nabla_d\Pi = \frac{\mathbf{g}\cdot\mathbf{d}}{c_p\theta}$ which gives no flow across the boundaries as long as the boundary faces are orthogonal ($\mathbf{d}\times\mathbf{S} = 0$ on the boundary). This can always be enforced by setting $\mathbf{d}$ to be parallel to $\mathbf{S}$ on the boundaries.

Using $U = HV$, equation (31) can now be substituted into the RHS of the continuity equation (2):

$$\begin{aligned}\rho^j &= \rho^1 - \alpha\Delta t\nabla\cdot\left(HV^j\right)\\ &= \rho^1 - \alpha\Delta t\nabla\cdot\left(HGV^{3M+1}\right) - \alpha\Delta t\nabla\cdot\left(HG\alpha\triangle t\rho_f^{j-1}\mathbf{g}\cdot\mathbf{d}\right)\\ &+ \alpha\Delta t\nabla\cdot\left(HG\alpha\Delta t c_p\rho_f^{j-1}\theta_f^{j-1/2}\nabla_d\Pi^j\right).\end{aligned} \tag{33}$$

To make this into a Helmholtz equation for Π^j, we need to replace ρ^j on the LHS with a linear function of Π^j. This can be done using the equation of state (5):

$$\rho^j = \Psi^j\,\Pi^j, \tag{34}$$

where

$$\Psi^j = \left(\rho^j\right)^{\frac{2\kappa-1}{\kappa-1}}\left(\frac{R\theta}{p_0}\right)^{\frac{\kappa}{\kappa-1}} \approx \left(\frac{p_0}{R}\right)^{0.4}\frac{\left(\rho^{j-1}\right)^{0.6}}{\left(\theta^{j-1}\right)^{0.4}}.$$

Because of the low powers of ρ and θ in Ψ (assuming that $\kappa = 1.4$), Ψ varies less than ρ and Π. Therefore the above linearisation is useful and leads to a convergent sequence (in the tests so far undertaken but analysis is needed). Substituting (34) into (33) gives the Helmholtz equation for Π^j:

$$\begin{aligned}\Psi^{j-1}\Pi^j = \Psi^1\Pi^1 &- \alpha\Delta t\nabla\cdot\left(HGV^{3M+1}\right) - (\alpha\Delta t)^2\nabla\cdot\left(HG\rho_f^{j-1}\mathbf{g}\cdot\mathbf{d}\right)\\ &+ (\alpha\Delta t)^2\nabla\cdot\left(HGc_p\rho_f^{j-1}\theta_f^{j-1/2}\nabla_d\Pi^j\right).\end{aligned} \tag{35}$$

This leads to a sparse, symmetric matrix which is solved using the conjugate gradient solver from OpenFOAM (cited 2013) with incomplete Cholesky preconditioning.

g. Back Substitution

Once (35) is solved for Π^j, V^j is updated from (31) (the back-substitution). Unlike in ENDGAME (Davies et al. 2005; Melvin et al. 2010), there is no back substitution for θ_f. Instead, final solutions of equations (21) and (22) are calculated for the beginning of the next time step.

h. Conservation and Consistency

Regardless of the level of convergence, this solution algorithm will always give exact local mass conservation. However, only at convergence will the density calculated from the continuity equation (2) equal the density calculated from the equation of state (34).

i. Alternative Model Formulations

In order to demonstrate the value of the novel aspects of the discretisation presented, two alternative approaches are presented and have been implemented for comparisons.

1) HORIZONTAL PRESSURE GRADIENT ($\partial p/\partial x$)

Most models of the global atmosphere use horizontal winds as prognostic variables and require reconstruction of horizontal pressure gradients (eg Klemp 2011; Zängl 2012). A similar approach is presented in order to compare with the new version which uses the H operator. This version is called $\partial p/\partial x$. In this form, U is the prognostic variable rather than V and V is infact not defined. The momentum equation is formulated in direction **S** rather than **d** (ie in the horizontal direction and in the near vertical direction, normal to cell faces). The derivation in direction **S** rather than **d** is very similar apart from the gradient at the face in direction **S**, $\nabla_s\Psi = \nabla\Psi\cdot\mathbf{S}$, which is given by a least squares fit to the linear polynomial:

$$\Psi = a + bx + cz$$

where the coefficients a, b and c are set using values of Ψ in stencils around each edge as shown in figure 2 and as described in Weller et al. (2009). This approach is not as sophisticated a form as that used by Zängl (2012) but it is a similar complexity to the H version so as to make a like for like comparison.

2) EXPLICIT SOLUTION OF GRAVITY WAVES

In order to treat gravity waves explicitly, acoustic waves implicitly and make no other changes to the formulation, $\theta_f = \theta_F$ is used instead of equations (26) and

$$G = \frac{1}{1+\alpha\Delta t\mu} \tag{36}$$

is used instead of equation (32).

3. Results

A number of test cases from Skamarock and Doyle (cited 2013) are used to demonstrate the value of the curl-free pressure gradient, the advection sub-cycling and the implicit treatment of gravity waves.

a. Resting Atmosphere

1) TEST CASE SETUP

We start with the simulation of a resting stratified atmosphere over a range of hills (Schär et al. 2002) using the test case setup of Klemp (2011). The lower boundary takes the form used by Schär et al. (2002):

$$h(x) = h_m\exp\left[-\left(\frac{x}{a}\right)^2\right]\cos^2\frac{\pi x}{\lambda} \tag{37}$$

where $a = 5$km, $\lambda = 4$km and $h_m = 1000$m. θ is set by specifying the Brunt–Väisälä frequency:

$$N = \begin{cases}0.01\text{s}^{-1} & 0\text{km} \le z \le 2\text{km and } 3km \le z \le 20\text{km}\\ 0.02\text{s}^{-1} & 2\text{km} \le z \le 3\text{km}\end{cases}$$

and $\theta(z=0) = 288$K. Π is initialised to be in discrete hydrostatic balance (in the vertical). The resolution is set to $\Delta x =$ 500m and $\Delta z = 500$m away from the terrain. The depths of the terrain following layer are set in two ways to compare with the results of Klemp (2011). First using basic terrain following (BTF) coordinates:

$$z = (z_t - h)\frac{\zeta}{z_t}$$

where z_t is the domain top and ζ is the layer height before orography is added. Next the layer depths are set to follow the SLEVE vertical coordinate (Schär et al. 2002) with decay functions specified following Leuenberger et al. (2010) with $s_1 =$ 4km and $s_2 = 1$km and $n = 1.35$. The domain is 20km in the x direction and 20km in the z direction with rigid boundaries at the top, bottom and sides. This domain is smaller than that used by Klemp (2011) in the x direction to reduce run times and the boundaries are rigid rather than open for simplicity. No sponge layer or diffusion are used. All test case results shown have implicit treatment of gravity waves but for the time-step used, the results are almost indistinguishable using the explicit gravity wave formulation.

2) Test Case Results

Entropy contours after 5 hours from the model using the new H formulation and the model using the $\partial p/\partial x$ formulation on the BTF and SLEVE grids, are presented in figure 4, all with implicit treatment of gravity waves. The advection scheme is not very diffusive and no explicit diffusion is used and so the simulation on the BTF grid using the $\partial p/\partial x$ formulation has very distorted θ contours. The distortions can be dramatically reduced by either using the H formulation or by using the SLEVE grid and using both makes the contours even flatter.

The maximum (spurious) vertical velocities generated for each of the model runs are shown in figure 5 where they are compared with the maximum vertical velocity from figure 4 of Klemp (2011) (note different y-scales). This shows that the $\partial p/\partial x$ formulation on the BTF grid generates the largest spurious vertical velocities and in the first hour, the erroneous velocities are higher than those of Klemp (2011). However on the BTF grid, the Klemp (2011) errors grow, unlike the $\partial p/\partial x$ and H errors on both grids. Use of either the SLEVE grid or the H version reduces the errors to a level similar to the results of Klemp (2011) on the SLEVE grid. It is intriguing that our results are less sensitive to the choice of grid than those of Klemp (2011). A conjecture is that our results have better energy conservation and so the errors do not grow whereas the Klemp (2011) results have better treatment of the boundary. Klemp (2011) uses quadratic interpolations at the boundary to maintain 2nd order accuracy whereas our results reduce to first order at the boundaries. With smaller truncation errors at the boundaries, Klemp (2011) errors do not jump up immediately after initialisation whereas for our model, errors are generated for both grids and both model versions at the boundaries initially but then do not grow.

The discretisation described in this paper does not give exact energy conservation therefore it is worth examining the energy conservation and the influence of the using the H operator on energy conservation. The normalised energy change from the initial conditions is defined to be $(E - E(0))/E(0)$, where $E = KE + PE + c_v \rho \theta \Pi$. This is shown in figure 6 for the simulations using the BTF grid and the SLEVE grid and for the simulations using the $\partial p/\partial x$ formulation and the H operator are . The energy conservation using the H formulation is at least an order of magnitude better than than using the $\partial p/\partial x$ version on the BTF grid. The dashed lines on the left of figure 6 show negative changes which implies that the H formulation loses energy which is desirable for stability. On the BTF grid, the contributing terms to the energy conservation are shown for both model versions in figure 6. Although the H version does not conserve energy to machine precision, the transfers between internal and potential energy on short time-scales are represented whereas they both increase in tandem for the $\partial p/\partial x$ version, leading to large energy increases. We are solving the flux form rather than vector invariant momentum equation and so the conservative transfer of energy to and from kinetic energy is not guaranteed.

b. Schär et al. (2002) Mountain Waves

1) Test Case Setup

The test case described by Schär et al. (2002) has flow over mountains with small and large features which are lower and less steep in comparison to those described in section a. The lower boundary has the same form (eqn 37) and again uses $a =$ 5km and $\lambda = 4$km but for this test case $h_m = 250$m. The initial conditions are set using $N = 0.01\text{s}^{-1}$ and a mean wind of $U =$ 10ms^{-1}. Schär et al. (2002) and Klemp et al. (2003) use a time step of 8s for this test case but following Melvin et al. (2010) we use a time step of 40s, corresponding to a horizontal Courant number of 0.8. Following Melvin et al. (2010) we use a domain of $100\text{km} \times 30\text{km}$, $\Delta x = 0.5$km, $\Delta z = 300$m, surface temperature of 288K and an absorbing layer in the top 10km of the domain with $\bar{\mu}\Delta t = 1.2$. The terrain is followed using both the BTF grid and the SLEVE grid. The upper and lower boundaries are rigid with zero flow. The inlet boundary has the prescribed θ profile and wind of $10\text{ms}^{-1}$and the outlet boundary is zero gradient. The boundary condition for Π is hydrostatic all around.

This is not a good case for testing the implementation of the implicit gravity waves since $N\Delta t = 0.4$ which is stable even if gravity waves are treated explicitly (Cullen 1990). The time-step cannot be further increased due to the explicit treatment of non-linear advection (although some increase could be acheived by substepping this term, this has not been done for this test case). The advection limits the time-step according to the multi-dimensional definition of Courant number for cell c:

$$Co_c = \frac{\Delta t}{2V_c \rho_c} \sum_{f \in c} U_f$$

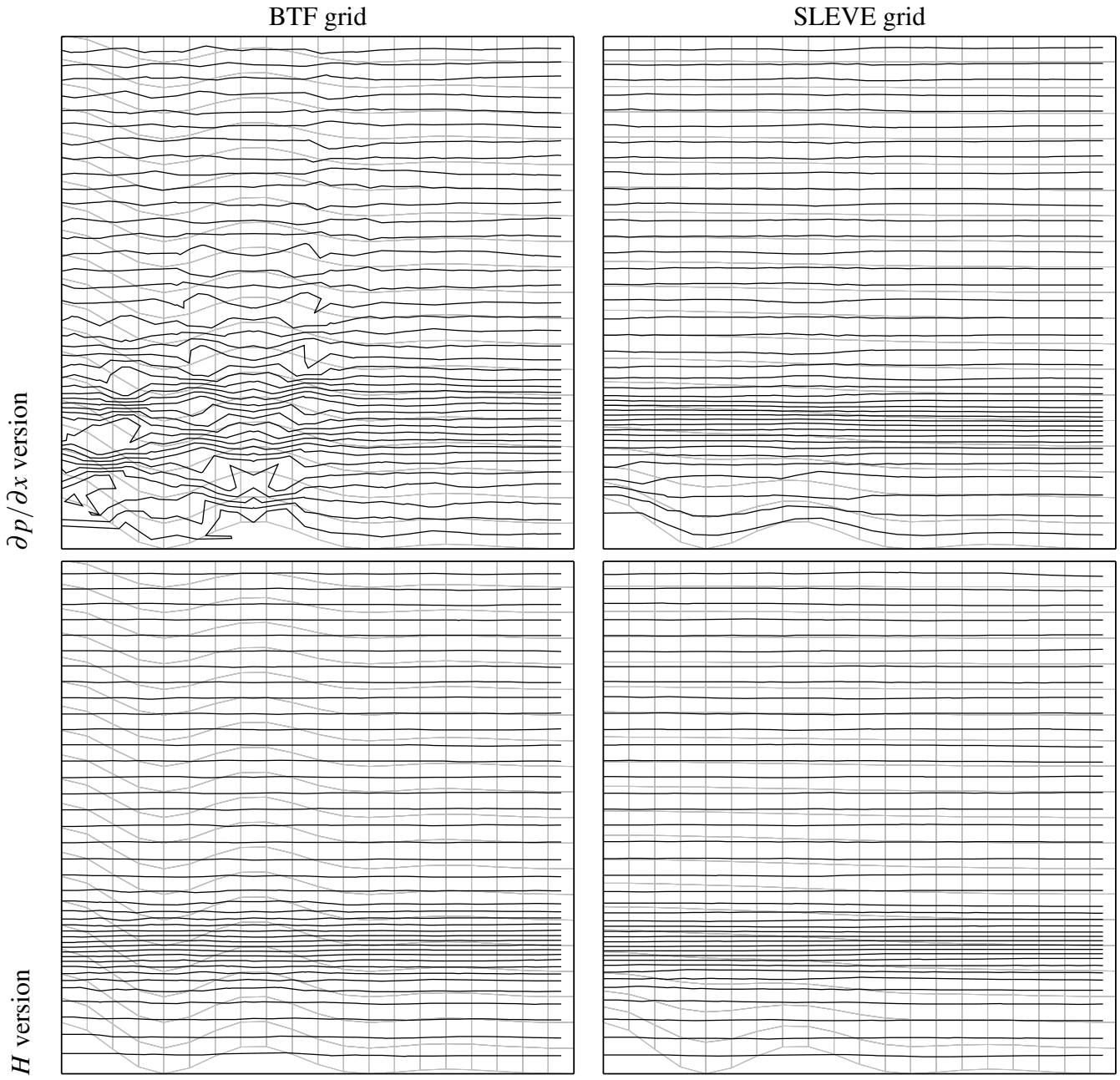

FIG. 4. Potential temperature contours (every 1K) after 5 hours for the resting stratified atmosphere over Schär et al. (2002) orography on two grids using two model formulations. The grids are shown in grey. All simulations use the formulation with implicit gravity waves, Δt=100s and a maximum $N\Delta t$=2. (Underground contours are created by the plotting package.)

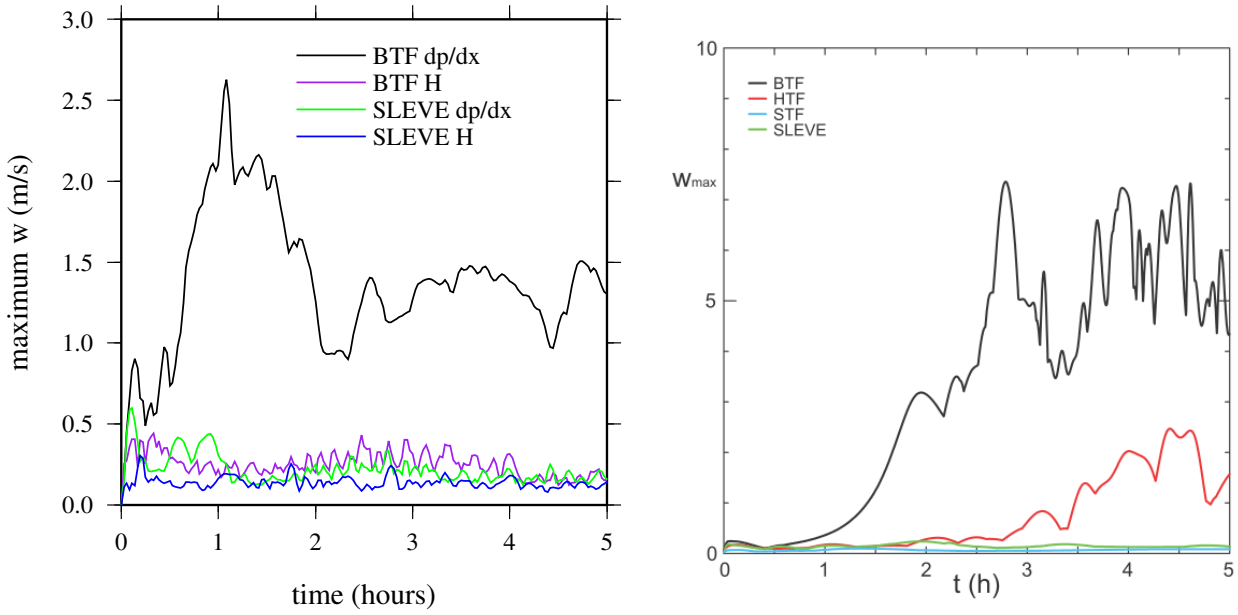

FIG. 5. Maximum vertical velocity for the resting stratified atmosphere over the Schär et al. (2002) orography on both grids and using both model formulations in comparison to figure 4 from Klemp (2011) (note different y-scales).

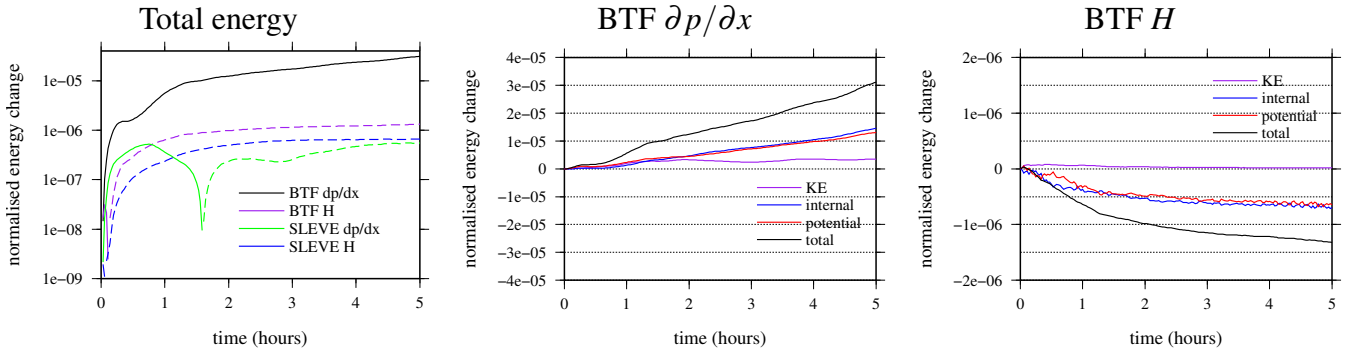

FIG. 6. Normalised energy change for the resting stratified atmosphere over the Schär et al. (2002) orography on both grids and using both model formulations (left). Negative energy changes on the log scale are dashed. Changes in kinetic, internal, potential and total energy for the H formulation on the BTF grid (right).

which has a maximum value of 1.04 for $\Delta t = 40$s for the initial conditions on the BTF grid.

2) TEST CASE RESULTS

The vertical velocities generated by the mountain are shown in figure 7 using both model versions ($\partial p/\partial x$ and H) with implicit gravity waves on the BTF and SLEVE grids. These are compared with the simulations from Melvin et al. (2010) and the analytic solution from Melvin et al. (2010). All four simulations give similar results but the $\partial p/\partial x$ version on the BTF grid has some noisy contours. The advection scheme we are using is not monotonic which allows these oscillations to form. However, for the other simulations which use the same advection scheme, no noisy contours are generated. Melvin et al. (2010) achieve almost perfect results using a time-step of 8s but their results using a time-step of 40s are shown in figure 7 to compare directly with our results.

c. Linear hydrostatic flow over a hill

1) TEST CASE SETUP

In order to demonstrate the value of having implicit gravity waves, it is necessary to go to coarser horizontal resolution to allow running with a longer time step and hence achieve larger $N\Delta t$. Decreasing the horizontal resolution makes the resolved flow closer to hydrostatic. The simultations of hydrostatic flow are done with the same non-hydrostatic model. The test case of hydrostatic mountain waves from Skamarock and Doyle (cited 2013) and used by Melvin et al. (2010) has a witch-of-Agnesi hill profile:

$$h(x) = \frac{h_m a^2}{x^2 + a^2}$$

with $h_m = 1$m (to ensure that the solution is close to linear), $a = 10$km, a mean wind speed of 20ms^{-1} and an initial isothermal temperature of $T = 250$K in discrete hydrostatic balance. Following Melvin et al. (2010), an absorbing layer is applied in the top 20km with $\bar{\mu}\Delta t = 0.3$. The domain is 240km wide, centered on the hill and 50km deep with mesh spacing $\Delta x = 2$km within 40km of the hill and increasing by a factor 1.1 to 10.5km at the lateral boundaries and $\Delta z = 250$m below 20km increasing by a factor 1.1 to 3070m at the top boundary. The fine resolution region is the same as the resolution used by Melvin et al. (2010). Time-steps of 20s, 100s and 200s are used giving Courant numbers of 0.2, 1 and 2 and $N\Delta t = 0.4$, $N\Delta t = 2$ and $N\Delta t = 4$ in order to demonstrate the value of the implicit gravity waves and the value of the advection sub-cycling. The cases with time-steps of 20s and 100s do not use advection sub-cycling. The case with the 200s time step and a maximum Courant number of 2 uses 2 sub time-steps for the advection and 3 rather than 2 final implicit stages. In order to increase the values of $N\Delta t$, a version with coarser resolution, by a factor of 2, in the horizontal and vertical is used. This coarser simulation uses a time step of 500s giving a maximum Courant number of 2.5, 3 sub time-steps for advection and 3 final implicit stage. The boundary conditions for all simulations are as described in section 1.

d. Test Case Results

Vertical velocity contours for the near hydrostatic flow over a hill are shown in figure 8 for model formulations using explicit and implicit gravity waves and the different time steps and spatial resolutions. The H and $\partial p/\partial x$ versions of the model are almost identical for this test case because the meshes are practically orthogonal with a hill height of only 1m. The numerical solutions are similar to the linear analytic, anelastic, non-hydrostatic solution (from Melvin et al. 2010) except slightly more wobbly ahead of and behind the mountain which is not understood but is sensitive to the advection scheme. The version with explicit gravity waves is stable for a time-step of 20s (corresponding to $Co = 0.2$, maximum $N\Delta t = 0.4$) but, unlike the version with implicit gravity waves, is not stable for a time-step of 100s (corresponding to $Co = 1$, maximum $N\Delta t = 2$). The version with implicit gravity waves can be run stably at much longer time steps, corresponding to Courant numbers of 2 and 2.5 with $N\Delta t = 4$ and $N\Delta t = 10$ (at coarser horizontal resolution and using sub-stepping for advection). At longer time-steps, the simulations remain stable (while never using more than 3 final implicit stages) but dramatically lose accuracy, likely because the potential temperature advection is handled implicitly whereas the non-linear advection is handled explicitly with sub stepping. It would be worth investigating handling all of the advection explicitly using sub stepping.

4. Discussion and Conclusions

A new semi-implicit model of the fully compressible Euler equations has been presented which has implicit treatment of acoustic and gravity waves, sub-cycling of advection and the use of co-variant components of velocity over orography which permits the calculation of curl-free pressure gradients. This is achieved solving all flux form equations in a finite volume model without mean and perturbation variables. These properties have enabled the following test case results:

- Simulation of a resting, stratified atmosphere over steep terrain with co-variant rather than contravariant prognostic velocities has lead to smaller spurious velocities, better energy conservation and a realistic transfer between potential and internal energy.
- Simulation of gravity waves over orography - both near hydrostatic and non-hydrostatic, are similar to previously published work. The implicit treatment of gravity waves, acoustic waves and θ advection and the sub-cylcing of non-linear advection means that the model can be run stably with long time steps. Results with advective Courant numbers of up to 2.5 and $N\Delta t$ of up to 10 are presented, which are only stable when using the code version with implicit gravity waves. Simulations with longer time steps

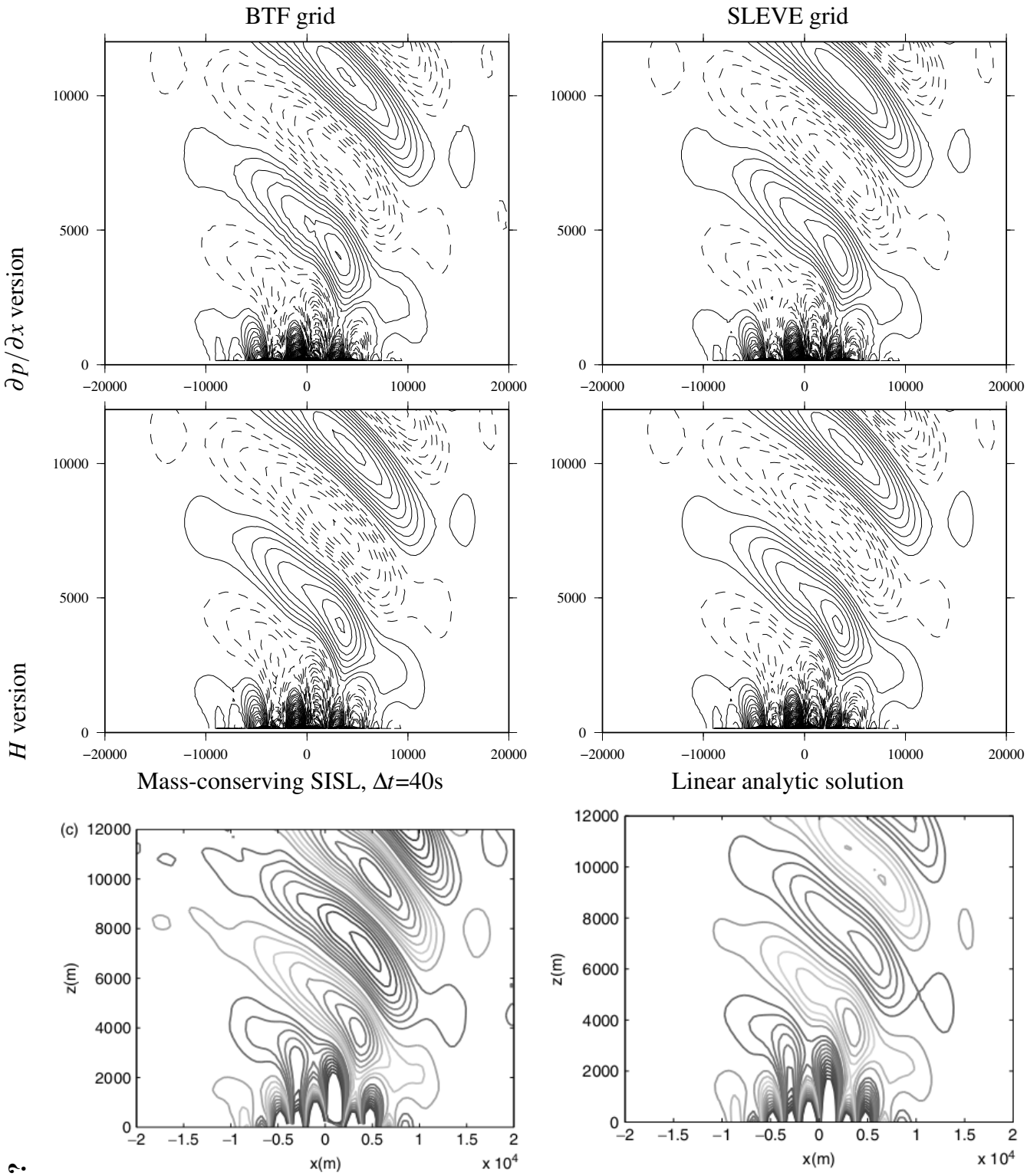

FIG. 7. Vertical velocity after 5 hours for the flow over a Schär et al. (2002) mountain on the BTF and SLEVE grids using both model version with implicit gravity waves. Contours 5×10^{-2}ms^{-1}, negative contours dashed, no zero contour. Δt=40s. Maximum $N\Delta t$=0.4. Compared with the results of Melvin et al. (2010) using mass-conserving SISL (their figure 7c) and with their linear analytic solution.

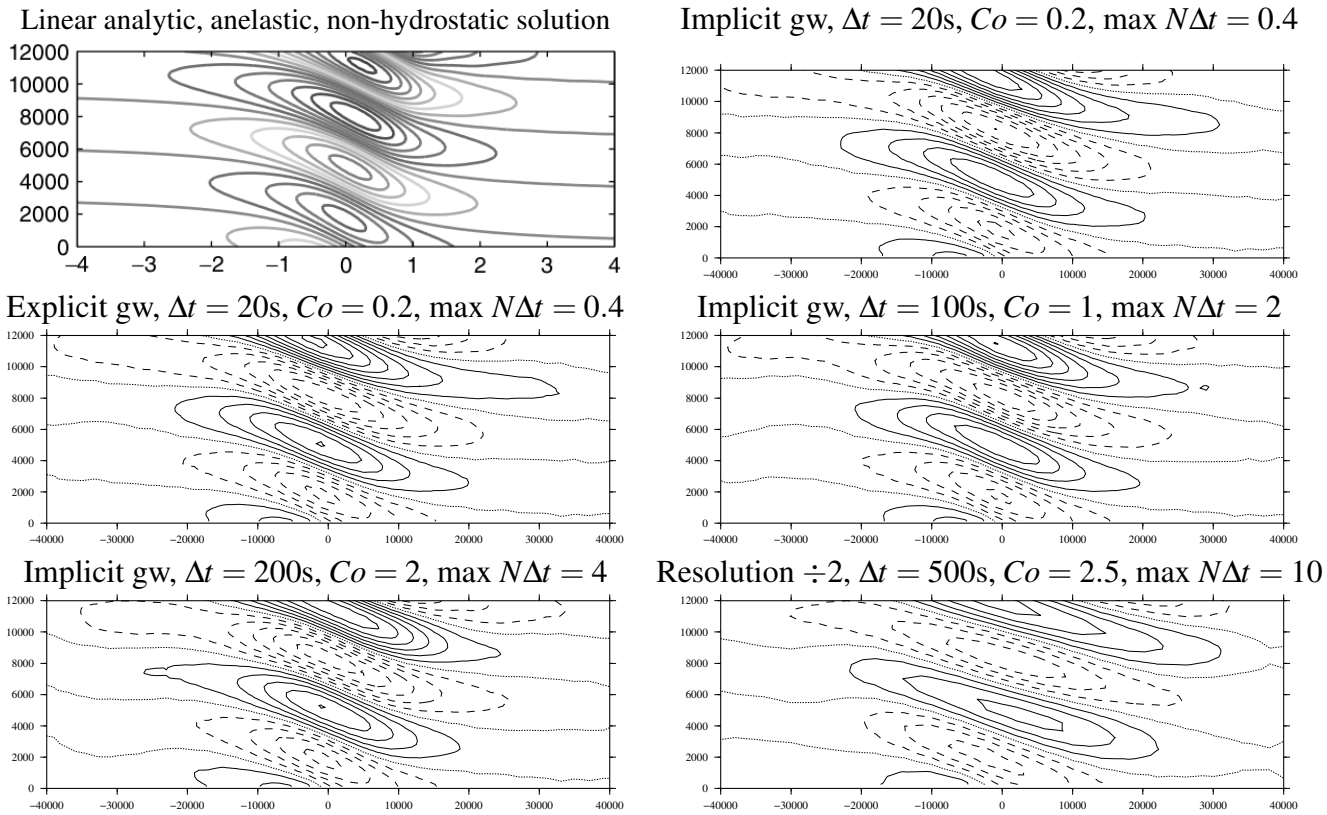

FIG. 8. Vertical velocity after 15,000 seconds for near hydrostatic flow over a hill using the H model formulations with implicit and explicit gravity waves (gw). The analytic solution is taken from figure 4e of Melvin et al. (2010). Contours 5×10^{-4}ms^{-1}, negative contours dashed, zero contour dotted.

are also stable but the results are not accurate due to the implicit θ advection. It is possible that the accuracy at large time-steps could be improved by sub-cylcing the θ advection rather than solving it implicitly but this has not been tried. The solution with implicit gravity waves has been presented, for the first time, without splitting variables into mean and perturbation quantities and using the flux form of the θ equation.

Three time-stepping schemes are combined to form a Runge-Kutta implicit-explicit-explicit (RK IMEXEX) scheme which is analysed and the combination of the 3 schemes is found to be stable. Using this framework, sub-cycling of advection enables longer time-steps but without a significant gain in efficiency since the non-linear advection term is expensive to calculate. However, since this term is calculated explicitly, it should be relatively straightforward to locally sub-cycle this term, in the region of large Courant numbers, in order to achieve dramatic efficiency gains by running with long time steps and similar accuracy to semi-Lagrangian. This again is a topic for future research.

5. Acknowledgements

Hilary Weller acknowledges support from NERC grant NE/H015698/1. Ava Shahrokhi acknowledges support from NERC grant NE/K006797/1. We also acknowledge useful discussions and ideas from John Thuburn, Nigel Wood, Colin Cotter and Tom Melvin.

REFERENCES

A. Adcroft, C. Hill, and J. Marshall. Representation of topography by shaved cells in a height coordinate ocean model. *Mon. Wea. Rev.*, 125:2293–2315, 1997.

A. Adcroft, J.-M. Campin, C. Hill, and J. Marshall. Implementation of an atmosphereâĂŞocean general circulation model on the expanded spherical cube. *Mon. Wea. Rev.*, 132(12): 2845–2863, 2004.

A. Arakawa and C. Konor. Vertical differencing of the primitive equations based on the Charney-Phillips grid in hybrid $\sigma - p$ vertical coordinates. *Mon. Wea. Rev.*, 124(3):511–528, 1996.

A. Arakawa and S. Moorthi. Baroclinic instability in vertically discrete systems. *J. of Atmos Sci.*, 45(11):1688–1707, 1988.

T. Benacchio, W. O'Neill, and R. Klein. A blended sound-proof-to-compressible numerical model for atmospheric dynamics. *Mon. Wea. Rev.*, submitted, 2014.

L. Bonaventura. A semi-implicit semi-lagrangian scheme using the height coordinate for a nonhydrostatic and fully elastic model of atmospheric flows. *J. Comput. Phys.*, 158(2):186–213, 2000.

M. Cullen. A test of a semi-implicit integration technique for a fully compressible nonhydrostatic model. *Quart. J. Roy. Meteor. Soc.*, 116(495):1253–1258, 1990. doi: {10.1002/qj.49711649513}.

M. Cullen and T. Davies. A conservative split-explicit integration scheme with fourth-order horizontal advection. *Quart. J. Roy. Meteor. Soc.*, 117(401):993–1002, 1991.

T. Davies, M. Cullen, A. Malcolm, M. Mawson, A. Staniforth, A. White, and N. Wood. A new dynamical core for the Met Office's global and regional modelling of the atmosphere. *Quart. J. Roy. Meteor. Soc.*, 131(608):1759–1782, 2005. doi: {10.1256/qj.04.101}.

D. Durran and J. Klemp. A compressible model for the simulation of moist mountain waves. *Mon. Wea. Rev.*, 111(12): 2341–2361, Dec 1983.

A. Gassmann. A global hexagonal C-grid non-hydrostatic dynamical core (ICON-IAP) designed for energetic consistency. *Quart. J. Roy. Meteor. Soc.*, 139(670):152–175, Jan 2013. doi: {10.1002/qj.1960}.

B. Good, A. Gadian, S.-J. Lock, and A. Ross. Performance of the cut-cell method of representing orography in idealized simulations. *Atmos. Sci. Lett.*, 2013.

L. Harris and S.-J. Lin. A two-way nested global-regional dynamical core on the cubed-sphere grid. *Mon. Wea. Rev.*, 141 (1):283–306, 2013.

D. Holdaway, J. Thuburn, and N. Wood. Comparison of Lorenz and Charney-Philips vertical discretisations for dynamics-boundary layer coupling. Part I: Steady states. *Quart. J. Roy. Meteor. Soc.*, 139, 2013.

Z. Janjic, J. Gerrity, and S. Nickovic. An alternative approach to nonhydrostatic modeling. *Mon. Wea. Rev.*, 129(5):1164–1178, 2001.

J. Klemp. A terrain-following coordinate with smoothed coordinate surfaces. *Mon. Wea. Rev.*, 139:2163–2169, 2011.

J. Klemp, W. Skamarock, and O. Fuhrer. Numerical consistency of metric terms in terrain-following coordinates. *Mon. Wea. Rev.*, 131(7):1229–1239, 2003.

J. Klemp, W. Skamarock, and J. Dudhia. Conservative split-explicit time integration methods for the compressible nonhydrostatic equations. *Mon. Wea. Rev.*, 135(10):2897–2913, 2007.

M. Kwizak and A. Robert. A semi-implicit scheme for grid point atmospheric models of the primitive equations. *Mon. Wea. Rev.*, 99(1):32–36, 1971.

D. Leuenberger, M. Koller, O. Fuhrer, and C. Schär. A new terrain-following vertical coordinate formulation for atmospheric prediction models. *Mon. Wea. Rev.*, 138(9):3683–3689, 2010.

S. Lock, N. Wood, and H. Weller. Numerical analyses of Runge-Kutta implicit-explicit schemes for horizontally-explicit vertically-implicit solutions of atmospheric models. *Quart. J. Roy. Meteor. Soc.*, accepted, 2013.

T. Melvin, M. Dubal, N. Wood, A. Staniforth, and M. Zerroukat. An inherently mass-conserving semi-implicit semi-Lagrangian discretisation of the nonhydrostatic vertical slice equations. *Quart. J. Roy. Meteor. Soc.*, 137:799–814, 2010.

R. Nair, S. Thomas, and R. Loft. A discontinuous galerkin global shallow water model. *Mon. Wea. Rev.*, 133(4):876–888, 2005.

OpenFOAM. The opensource CFD toolbox. [Available online at `http://www.openfoam.org`], cited 2013. The OpenCFD Foundation.

L. Pareschi and G. Russo. Implicit-explicit Runge–Kutta schemes and application to hyperbolic systems with relaxation. *J. Sci. Comp.*, 25(1/2):129–155, 2005. doi: 10.1007/s10915-004-4636-4.

W. Putman. *Development of the Finite-Volume Dynamical Core on the Cubed-Sphere*. PhD thesis, The Florida State University, 2007. Electronic Theses, Treatises and Dissertations. Paper 511.

J. Qian, F. Semazzi, and J. Scroggs. A global nonhydrostatic semi-lagrangian atmospheric model with orography. *Mon. Wea. Rev.*, 126(3):747–771, 1998.

M. Rančić, R. Purser, and F. Mesinger. A global shallow-water model using an expanded spherical cube: Gnomonic versus conformal coordinates. *Quart. J. Roy. Meteor. Soc.*, 122(532), 1996.

M. Satoh, T. Matsuno, H. Tomita, H. Miura, T. Nasuno, and S. Iga. Nonhydrostatic icosahedral atmospheric model (nicam) for global cloud resolving simulations. *J. Comput. Phys.*, 227(7):3486–3514, 2008.

C. Schär, D. Leuenberger, O. Fuhrer, D. Lüthi, and C. Girard. A new terrain-following vertical coordinate formulation for atmospheric prediction models. *Mon. Wea. Rev.*, 130(10):2459–2480, 2002.

W. Skamarock and J. Doyle. Standard test set for nonhydrostatic dynamical cores of NWP models. [`http://www.mmm.ucar.edu/projects/srnwp\_tests`], cited 2013.

W. Skamarock and J. Klemp. The stability of time-split numerical methods for the hydrostatic and the nonhydrostatic elastic equations. *Mon. Wea. Rev.*, 120:2109–2127, 1992. doi: {10.1175/1520-0493(1992)120<2109:TSOTSN>2.0.CO;2}.

P. Smolarkiewicz and J. Szmelter. A nonhydrostatic unstructured-mesh soundproof model for simulation of internal gravity waves. *Acta Geophysica*, 2011. doi: {10.2478/s11600-011-043-z}.

P. Smolarkiewicz, L. Margolin, and A. Wyszogrodzki. A class of nonhydrostatic global models. *J. of Atmos Sci.*, 58(4):349–364, 2001.

P. Smolarkiewicz, C. Kühnlein, and N. Wedi. A unified framework for integrating soundproof and compressible equations of all-scale atmospheric dynamics. In *Recent developments in numerical methods for atmosphere and ocean modelling*, ECMWF Annual Seminar, `http://www.ecmwf.int/newsevents/meetings/annual\_seminar/2013/index.html`, 2-5 Sept 2013. ECMWF.

J. Steppeler, H. Bitzer, M. Minotte, and L. Bonaventura. Nonhydrostatic atmospheric modelling using a z-coordinate representation. *Mon. Wea. Rev.*, 130(8):2143–2149, 2002.

J. Steppeler, R. Hess, U. Schattler, and L. Bonaventura. Review of numerical methods for non-hydrostatic weather prediciton models. *Meteorology and Atmospheric Physics*, 82(1-4):287–301, 2003.

M. Tanguay, A. Robert, and R. Laprise. A semi-implicit semi-Lagrangian fully compressible regional forecast model. *Mon. Wea. Rev.*, 118:1970–1980, 1990.

M. Tapp and P. White. A non-hydrostatic mesoscale model. *Quart. J. Roy. Meteor. Soc.*, 102(432):277–296, 1976. doi: {10.1002/qj.49710243202}.

J. Thuburn and C. Cotter. A framework for mimetic discretization of the rotating shallow-water equations on arbitrary polygonal grids. *SIAM Journal on Scientific Computing*, 34(3):B203–B225, 2012.

J. Thuburn, C. Cotter, and T. Dubos. A mimetic, semi-implicit, forward-in-time, finite volume shallow water model: comparison of hexagonal-icosahedral and cubed sphere grids. *Geosci. Model Dev.*, in prep, 2013.

P. Ullrich and C. Jablonowski. Operator-split Runge-Kutta-Rosenbrock methods for nonhydrostatic atmospheric models. *Mon. Wea. Rev.*, 140(4):1257–1284, 2012. doi: {10.1175/MWR-D-10-05073.1}.

H. Weller. Non-orthogonal version of the arbitrary polygonal C-grid and a new diamond grid. *Geosci. Model Dev.*, in discussion, 2013.

H. Weller, H. Weller, and A. Fournier. Voronoi, Delaunay and block structured mesh refinement for solution of the shallow water equations on the sphere. *Mon. Wea. Rev.*, 137(12):4208–4224, 2009.

H. Weller, S.-J. Lock, and N. Wood. Runge-Kutta IMEX schemes for the horizontally explicit/vertically implicit (HEVI) solution of wave equations. *J. Comput. Phys.*, 252: 365–381, 2013.

P. White. IFS documentation. Part III: dynamics and numerical procedures. Technical Report CY23R4, ECMWF, `http://www.ecmwf.int/research/ifsdocs\_old/DYNAMICS/index.html`, 2003.

G. Zängl. Extending the numerical stability limit of terrain-following coordinate models over steep slopes. *Mon. Wea. Rev.*, 140:3722–3733, 2012.

H. Zhu and R. Smith. Effects of vertical differencing in a minimal hurricane model. *Quart. J. Roy. Meteor. Soc.*, 129:1051–1069, 2003.